Simulations and analysis of high-temperature proton exchange membrane fuel cell and its cooling system to power an automotive vehicle

Runqi Zhu[1], Lu Xing[2, *, **], Zhengkai Tu[3, ***]

[1]China-EU Institute for Clean and Renewable Energy, Huazhong University of Science & Technology, Wuhan, 430074, China

[2]Mechanical and Construction Engineering, Northumbria University, Newcastle upon Tyne, NE1 8ST, United Kingdom

[3]School of Energy and Power Engineering, Huazhong University of Science and Technology, Wuhan, 430074, China

**Corresponding author: lu.xing@northumbria.ac.uk

Abstract:

Proton exchange membrane fuel cell, which utilizes mainly hydrogen for fuel, has many advantages for vehicle applications. Compared to conventional low-temperature proton exchange membrane fuel cell (60-80 °C), high-temperature fuel cell (120-180°C) requires a simpler system. It is characterized by enhanced electrochemical kinetics and can use liquid fuel such as methanol due to higher carbon monoxide tolerance. In this paper, phosphoric acid doped high-temperature proton exchange membrane fuel cell with a reformer system is applied for powering an automotive vehicle. Thermal management and control of the fuel cell stack for performance optimization remain critical. This paper aims to analyze the heat dissipation requirement for high-temperature fuel cell vehicles and propose cooling strategies for optimizing the performance. A simulation model of the high-temperature proton exchange membrane fuel cell stack and its oil cooling system were developed. The stack model had been validated against experimental results. The case study results show that increasing carbon monoxide concentration will increase the voltage loss. Increased operating temperature to 448K reduces the stack heat generation due to the poisoning effect. It is suggested to keep the inlet cooling oil temperature constant within the range of 435-445K and adjust the cooling oil flow rate (2.5-5kg/s) to meet the heat dissipation requirement for the fuel cell stack. Due to the significant temperature difference between the fuel cell and the external environment (> 150K), the recoverable waste heat is about 39kW.

Keywords: Proton exchange membrane fuel cell; High temperature; Phosphoric acid doped; Automotive vehicle; Reformer; Oil cooling

1. Introduction

Proton Exchange Membrane Fuel Cell (PEMFC), which utilizes mainly hydrogen for fuel, has many advantages for automotive applications [1], including high power density, efficiency, and rapid start-up. The commonly used Low-Temperature (LT) PEMFC (60-80 °C) is sensitive to Carbon Monoxide (CO) poisoning and must be coupled with a complex water management system [2]. The phosphoric acid doped High-Temperature (HT) PEMFC (120-180°C) is proposed for overcoming these challenges [3]. It was developed to meet the performance, durability, and cost targets required for the application [4]. Utilizing an HT PEMFC as a range extender for a full electric vehicle was analyzed [5]. Characterized by enhanced electrochemical kinetics and higher CO tolerance, they can use liquid fuel such as methanol, ethyl alcohol. Thermal management and control of the fuel cell remain critical for applying HT PEMFC for vehicles [6]. It plays a crucial role in efficiency optimization, fuel cell life span, and operational safety.

1.1 High-temperature proton exchange membrane fuel cell

Models of HT PEMFC stacks coupled with thermodynamic, kinetic, and resistance effects were developed. Li et al. [7] developed a HT PEMFC model and optimized the stack performance based on the particle swarm optimization algorithm. Li et al. [8] tested the CO tolerance of HT-PEMFC around 125-200°C and presented the stack performance. Mamlouk et al. [9] described a one-dimensional model which considers CO poisoning. Since the CO tolerance of electrocatalysts increases 3–5% at temperatures above 140 °C, HT-PEMFC can use syngas, a mixture of carbon oxides, hydrogen, and water as fuel. Researchers proposed to produce

hydrogen reformed from methanol or others; microreactor is one of the attractive configurations for reforming. The microreactor has a high surface area-to-volume ratio; its size satisfies laminar flow and low-pressure drop conditions. The miniaturization strategies reduce the equipment's size and weight while improving the heat and mass transfer performance [10]. A shorter residence time (<0.1 s) will result in a faster dynamic response under inlet conditions, which will immediately affect the system [11]. For modeling the reforming process, Chodba et al. [12] proposed a microreactor reformer system for providing reformer gas to HT-PEMFC. Suthida et al. [13] proposed a PEMFC model with a glycerol reformer. Unchalee et al. [14] investigated a model of PEMFC and sorption enhanced water gas shift reactor analyzed the effects of calcium oxide /carbon ratio, fuel utilization, and anode split ratio. Anders et al. [15] implemented a steam-reforming reactor, burner, and heat reservoir model and evaluated dynamical control strategies.

1.2 Thermal management

Previous research focused on the thermal management of LT PEMFC. The fundamental heat transfer mechanisms at the component level (including electrolyte, catalyst, gas diffusion layer, and bipolar plate) were reviewed [16]. The vehicle integrated thermal management system had been modeled, and control strategies were proposed [17]. A methodology for fault diagnosis of the thermal management system for the LT PEMFC has been proposed to ensure the system's reliability [18]. Different cathode flow channel configurations have been applied to improve fuel cell performance [19]. Sangseok et al. [20] established a fuel cell system model with a cooling module. They found that a feedback control algorithm is more suitable for a cooling

module than a convent control algorithm. Hosseinzadeh et al. [21] proposed water and thermal management approach to assess cooling inlet and outlet temperatures and the effects of temperature gradients. Zhang et al. [22] established a thermal management system model to predict the stack's performance. They gave a relationship between the output power of the stack, the flow rate of cooling water, the flow rate of the air intake, and the ambient temperature under steady conditions. Li et al. [23] estimate the disturbance using the extended state observer and stabilize the PEMFC temperature through active disturbance rejection control. Binrui et al. [24] designed a PEMFC temperature control module with fuzzy incremental Proportional–Integral–Derivative (PID) and conducted experiments on the designed control to achieve relatively stable temperature control. Cheng et al. [25] used feedforward and feedback control to control the cooling water temperature of urban buses based on the model.

There was research on thermal management of the HT PEMFC for a low power range (1-10kW). There are three methods for cooling: air cooling, liquid cooling, and phase change cooling [26]. PEMFC, which is less than 1kW, can be cooled by air. Sasiwimonrit and Chang [27] proposed thermal management of the HT PEMFC using air cooling and flatted heat pipes. Reddy and Jayanti [28] cooled a 1kW stack using forced convection and excess stoichiometric factors. Renau et al. [29] manufactured a 1.1kW air-cooling stack used in the unmanned aerial vehicle. The fuel cell can maintain a stable temperature when flying at a high altitude through the airflow field design. Liquid cooling is usually used in large-scale PEMFC; HT PEMFC can't use water as a coolant since they operate at over 100°C. Supra et al. [30] achieved an 8.3°C temperature difference from cell to cell through an oil cooling system. Ahrae et al. [31] tested a 5kW HT-

PEMFC system with a reforming reactor, and the waste heat from PEMFC was carried by triethylene glycol. Scholta et al. [32] maintained the temperature of a PEMFC through heat transfer liquid. Phase change cooling is another system that can be used in PEMFC. Song et al. [33] proposed a cooling device to be used for HT-PEMFC; the latent heat of water cooled the PEMFC without any external driving power. It has a simple cooling system and high capacity but is hard to control.

1.3 Research gap analysis

The previous research focused mainly on LT PEMFC for vehicles applications and its water-cooling system. Very few studies were performed for detailed analysis of the HT PEMFC stack performance when used for powering the automotive. There is rarely research about the thermal management system of the HT PEMFC vehicle. Few HT PEM FC stack models have been proposed in the previous study. Mamlouk et al. [9] proposed and validated a model against the experimental data collected. This model has been applied in the system model. Chodba et al. [12] proposed a reformer system to provide reformer gas to HT PEMFC. The reformer system and gas composition are used for the simulation considering the reformed gas composition ratio is constant. The cooling system proposed in previous research is either for different vehicles (truck, bus, etc.) or for automotive with a low power range (1-10kW). In all, the study of the thermal management system (30kW) for HT PEMFC for an automotive vehicle is lacking.

This paper investigates the feasibility of the HT PEMFC (30kW) with an oil cooling system applied in automobiles. A phosphoric acid-doped HT PEMFC stack simulation model was developed and validated. An oil cooling system is proposed for the thermal management of the

fuel cell stack. This paper aims to study the heat dissipation requirement for the HT PEMFC fuel cell vehicles, investigate the feasibility, and propose cooling strategies to optimize stack performance.

2. Methods

Fig. 1 presents the schematic of the PEMFC with reformer system on automotive vehicles. The system is composed of a PEMFC stack, a reformer system with the combustion chamber, methanol and water tank with pumps, air compressor, and cooling system (oil pump and radiator). Air is first compressed in the compressor. High pressure and high-temperature air is divided into two streams by the control of the valve. One part enters the cathode of the HT-PEMFC stack, and the other enters the reforming system, where it reacts with methanol to provide the heat required for the steam reforming process. The water and methanol are supplied into the reformer system and compounded the reformer gas transported to the anode of the stack. The exhaust gas from the anode mixes with the air and burn in the combustion chamber. The stack operating temperature is regulated by controlling the inlet cooling oil temperature and cooling oil flow rate. The cooling oil will be pumped and exchanged heat with environmental air in the radiator by forced convection. Then the cooling water returns to the stack to absorb heat.

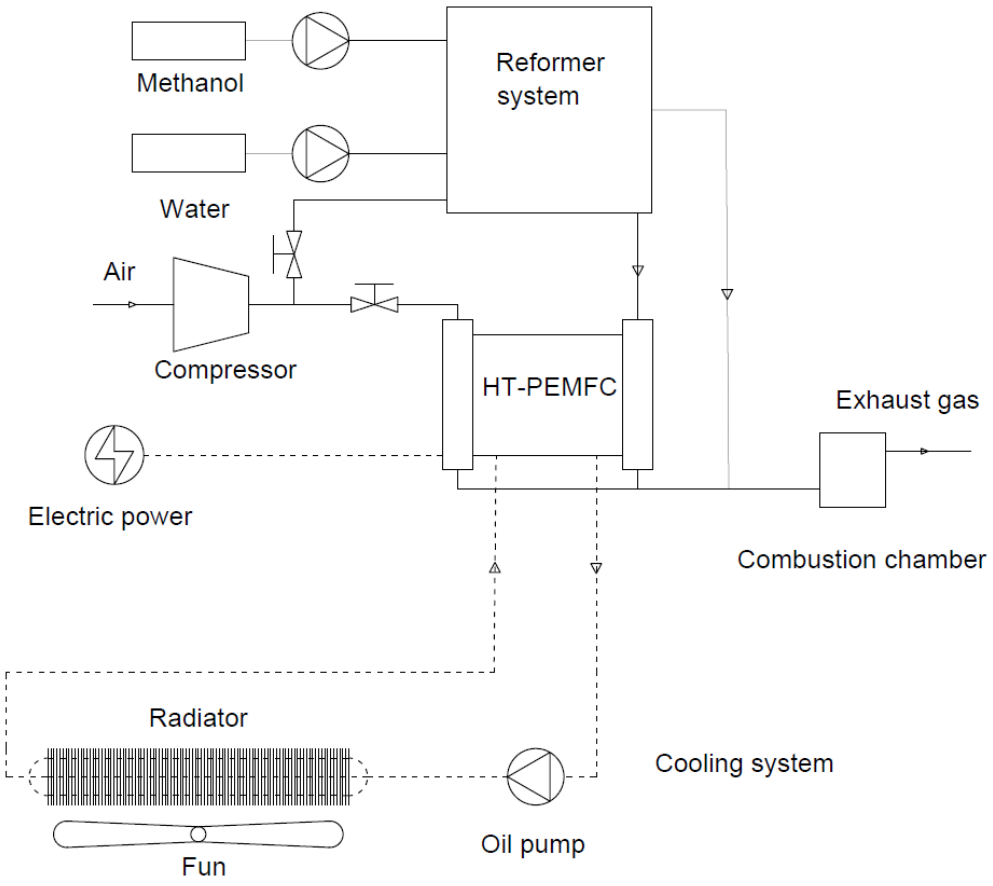

Fig. 1. High-temperature PEMFC stack integrated oil cooling and reformer system.

2.1 Fuel cell stack model

The one-dimensional fuel cell model includes two diffusion layers, the anode and cathode catalyst layers and the membrane. The gas flow channels are not considered. The overall cell voltage is given from a combination of the thermodynamic cell potential and voltage losses associated with Ohmic resistances in the electrodes and membrane and kinetic losses at the anode and cathode, which are influenced by mass transport restriction, Eq. (1):

$$V_{cell} = E_N - V_{act,a} - V_{act,c} - V_{ohmic} \quad (1)$$

Where, V_{cell} is the voltage of fuel cell (V); E_N is the Nernst voltage (V), given in Eq. (3); $V_{act,a}$ *and* $V_{act,c}$ are activation voltage of anode and cathode (V), given in Eq (19) and Eq. (20);

V_{ohmic} is the ohmic voltage loss (V), given in Eq. (24). The overall electrochemical reaction in an HT-PEMFC running on hydrogen (H_2) as fuel and Oxygen (O_2) as an oxidant can be shown in Eq. (2):

$$H_2 + \frac{1}{2}O_2 \overset{Pt}{\rightarrow} H_2O_{(g)} \tag{2}$$

The thermodynamic equilibrium potential can be calculated using the Nernst equation, Eq. (3):

$$E_N = -\left(\frac{\Delta H}{nF} - \frac{T\Delta S}{nF}\right) + \frac{RT}{nF}\ln\left[\frac{(RT)^{1.5}C_{Pt,H_2}C_{Pt,O_2}^{0.5}}{a_{H_2O}}\right] \tag{3}$$

Where the enthalpy ΔH (J/kg) and entropy ΔS (J/K·kg) are given in Eq. (4) and Eq. (5) [34], R is gas constant, 8.314 (J $\text{mol}^{-1}\text{K}^{-1}$), T is cell temperature (K), n is number of electrons involved in the reaction (unitless), F is faraday constant, 96485 (C mol^{-1}), H_2 or O_2 concentration on the catalyst surface C_{Pt,H_2} or C_{Pt,O_2} ($\text{mol}\,cm^{-3}$) are given in Eq. (7) and Eq. (8), and water activity a_{H_2O} (unitless) is given in Eq. (6) [35]:

$$\Delta H = -238.41 - 0.012256T + 2.7659 \times 10^{-6}T^2 \tag{4}$$

$$\Delta S = -18.449 - 0.01283T \tag{5}$$

$$a_{H_2O} = \frac{P_{H_2O}}{P^*_{H_2O}} = \frac{RH\%}{100} \tag{6}$$

Where T is cell temperature (K), P_{H_2O} is the water vapor pressure in equilibrium with the acid electrolyte (atm), $P^*_{H_2O}$ is the saturation vapor pressure of pure water at the same temperature (atm), RH is relative humidity(unitless). Eq. (7) and Eq. (8) present calculations of the oxygen/hydrogen concentration at the catalyst surface derived from Fick's law from oxygen and hydrogen diffusion:

$$C_{Pt,O_2} = C_{O_2}^{dissolved} - \frac{N_{O_2}\delta_{cathode}}{S_{Pt-cathode}D_{O_2}^{H_3PO_4}} \tag{7}$$

$$C_{Pt,H_2} = C_{H_2}^{dissolved} - \frac{N_{H_2}\delta_{anode}}{S_{Pt-anode}D_{H_2}^{H_3PO_4}} \quad (8)$$

Where H_2 and O_2 equilibrium concentration $C_{O_2}^{dissolved}$, $C_{H_2}^{dissolved}$ ($\mathrm{mol}\ cm^{-3}$) are given in Eq. (12) and Eq. (17) , $\delta_{cathode}$ and δ_{anode} are average film thickness of cathode and anode (m), $S_{Pt-cathode}$ and $S_{Pt-anode}$ are real platinum surface area on cathode and anode (m^2), diffusion coefficient of oxygen or hydrogen in phosphoric acid $D_{O_2}^{H_3PO_4}$ or $D_{H_2}^{H_3PO_4}$ (cm^2s^{-1}) are given in Eq. (11) and Eq. (18), species' flux N_{O_2} and N_{H_2} ($\mathrm{mol}\ s^{-1}m^{-2}$) can be given as Eq. (9) and Eq. (10):

$$N_{O_2} = \frac{i}{4F} \quad (9)$$

$$N_{H_2} = \frac{i}{2F} \quad (10)$$

Where i is current density($\mathrm{A\ cm^{-2}}$), F is faraday constant, 96485 ($\mathrm{C\ mol^{-1}}$). The oxygen solubility and diffusivity in hot phosphoric acid exhibit exponential reciprocal temperature dependencies in Eq. (11) and Eq. (12) [36]:

$$D_{O_2}^{H_3PO_4} = x\exp\left(-\frac{E_a}{RT}\right) \quad (11)$$

$$C_{O_2}^{dissolved} = y\exp(-\frac{\Delta H_{O_2}^{solu}}{RT}) \quad (12)$$

Where E_a is activation energy ($\mathrm{J\ mol^{-1}}$), $\Delta H_{O_2}^{solu}$ is the enthalpy of oxygen phosphoric acid solutions($\mathrm{J\ mol^{-1}}$). The activation energy of oxygen in phosphoric acid and oxygen enthalpy of solution at different acid weight concentrations (W) are calculated in Eq. (13) and Eq. (14):

$$E_a(J\ mol^{-1}) = 4185(-0.0116W^2 + 1.964W - 75.376) \quad (13)$$

$$\Delta H_{O_2}^{solu}(J\ mol^{-1}) = 4185(-0.00313W^3 + 0.837W^2 - 74.952W + 2244.8) \quad (14)$$

Where the pre-exponential factors of x and y are given as Eq. (15) and Eq. (16) [36]:

$$x = 2953780\exp(-0.2162766W) \quad (15)$$

$$\frac{1}{y} = 0.0004(1-W)^5 - 0.017(1-W)^4 + 0.25(1-W)^3 \quad (16)$$
$$- 1.71(1-W)^2 + 5.8(1-W) - 7.66$$

Hydrogen solubility was considered similar to that of oxygen at the same conditions (pressure, temperature, and phosphoric acid concentration) as Eq. (17) [9]. Similarly, the hydrogen diffusion coefficient in the phosphoric acid electrolyte can be written as Eq. (18) [9]:

$$C_{H_2}^{dissolved} = C_{O_2}^{dissolved} \quad (17)$$

$$D_{H_2}^{H_3PO_4} = 4D_{O_2}^{H_3PO_4} \quad (18)$$

The activation voltage loss of anode and cathode were given by Eq. (19) and Eq. (20) [14]:

$$V_{act,a} = \frac{RT}{\alpha_a F} sinh^{-1}\left(\frac{i}{2i_{0,a}(1-\theta_{CO})^2}\right) \quad (19)$$

$$V_{act,c} = \frac{RT}{\alpha_c F} sinh^{-1}\left(\frac{i}{2i_{0,c}}\right) \quad (20)$$

Where α_a and α_c are catalyst loading of anode and cathode; exchange current density at anode or cathode, $i_{0,a}$ or $i_{0,c}$ (A cm^{-2}) can be calculated by Eq. (21) and Eq. (22) [14]:

$$i_{0,a} = i_{0,a}^{ref} a_{c,a} L_{c,a} \left(\frac{C_{Pt}}{C_{ref,a}}\right)^{\gamma a} \exp\left[-\frac{E_{c,a}}{RT}\left(1 - \frac{T}{T_{ref,a}}\right)\right] \quad (21)$$

$$i_{0,c} = i_{0,c}^{ref} a_{c,c} L_{c,c} \left(\frac{C_{Pt}}{C_{ref,c}}\right)^{\gamma c} \exp\left[-\frac{E_{c,c}}{RT}\left(1 - \frac{T}{T_{ref,c}}\right)\right] \quad (22)$$

Where parameters in Eq. (21) and Eq. (22) can be found in Table 1. The CO coverage is developed from experimental data to explain a CO poisoning effect on PEMFC, which can be described as Eq. (23) [13]:

$$\theta_{CO} = a \cdot \ln\frac{|CO|}{|H_2|} + b \cdot \ln(i) \cdot \ln\frac{|CO|}{|H_2|} + c \quad (23)$$

$$\text{a} = -0.00012784T^2 + 0.11717499T - 26.62908873$$

$$b = 0.0001416T^2 - 0.12813608T + 28.852463626$$

$$c = -0.00034886T^2 + 0.31596903T - 70.11693333$$

The ohmic loss voltage can be calculated by Eq. (24):

$$V_{ohmic} = \left(\frac{l_m}{\delta_m}\right) i \tag{24}$$

Where l_m is the membrane thickness (m); δ_m is the film thickness (m), which can be found in Table 1. Eq. (25) calculate the proton conductivity σ_m (S cm^{-1}) of acid PBI membrane at different temperatures [9]:

$$\sigma_m = \frac{A}{T} \exp\left(\frac{-B}{R(T - 273.15)}\right) \tag{25}$$

The corresponding constants to calculate A and B are given as Eq. (26) and Eq. (27):

$$A = \exp(k_1^a RH^3 + k_2^a RH^2 + k_3^a RH + k_0^a) \tag{26}$$

$$B = \exp(k_1^b RH^3 + k_2^b RH^2 + k_3^b RH + k_0^b) \tag{27}$$

Where k_0^a is 9.6082; k_1^a is 0.0002; k_2^a is -0.0132; k_3^a is 0.2257; k_0^b is 26300; k_1^b is 0.62; k_2^b is -39.7; k_3^b is 527. Table 1 shows the parameters of the HT-PEMFC model.

Table 1 Physical and material property parameters for HT-PEMFC

Parameters	**Value**	**Units**
Faraday constant, $\boldsymbol{F}$	96485	C mol^{-1}
Active area, $\boldsymbol{A}$	200	cm^2
Number of cells, $\boldsymbol{n}$	400	N/A
Membrane thickness, $\boldsymbol{l_m}$	4×10^{-5}	m
Anode film thickness, $\boldsymbol{\delta_{anode}}$	2.5×10^{-9}	m
Cathode film thickness, $\boldsymbol{\delta_{cathode}}$	1.48×10^{-9}	m

Anode reference exchange current density, $i_{0,a}^{ref}$	1440	A m^{-2}
Cathode reference exchange current density, $i_{0,c}^{ref}$	0.0004	A m^{-2}
Anode catalyst surface area, $a_{c,a}$	64	m^2 g^{-1}
Cathode catalyst surface area, $a_{c,c}$	32.25	m^2 g^{-1}
Anode catalyst loading, $L_{c,a}$	0.0002	g cm^{-2}
Cathode catalyst loading, $L_{c,c}$	0.0004	g cm^{-2}
Transfer coefficient at anode, α_a	0.5	N/A
Transfer coefficient at cathode, α_c	0.75	N/A
Reaction order at anode, γa	1	N/A
Reaction order at cathode, γc	1.375	N/A
Anode reference concentration, $C_{ref,a}$	2×10^{-7}	mol cm^{-3}
Cathode reference concentration, $C_{ref,c}$	4×10^{-7}	mol cm^{-3}
Anode activation energy, $E_{c,a}$	16900	J mol^{-1} K^{-1}
Cathode activation energy, $E_{c,c}$	72400	J mol^{-1} K^{-1}
Anode reference cell temperature, $T_{ref,a}$	433.15	K
Cathode reference cell temperature, $T_{ref,c}$	373.15	K

2.2 Reformer

A reformer system with multiple heat exchangers, as shown in Fig. 2 is used. The methanol and water are pressurized by the pump, they are mixed and passed through the Heat Exchanger 1(HEX1) and the Heat Exchanger 2 (HEX2), respectively. They are heated by the high-temperature gas at the outlet of the reformer, then become high-temperature steam and enter the

steam reforming passage of the reformer. The other part of methanol is heated by the Heat Exchanger 3 (HEX3) and mixed with compressed air into the Heat Exchanger 4(HEX4), then enters the oxidation channel of the reformer. The oxidation process provides heat, and its exhaust gas enters HEX3 and HEX4 for heat exchange. Both reforming waste gas and fuel cell exhaust gas will enter the combustion chamber, enter the HEX2 for heat exchange, and be discharged into the atmosphere.

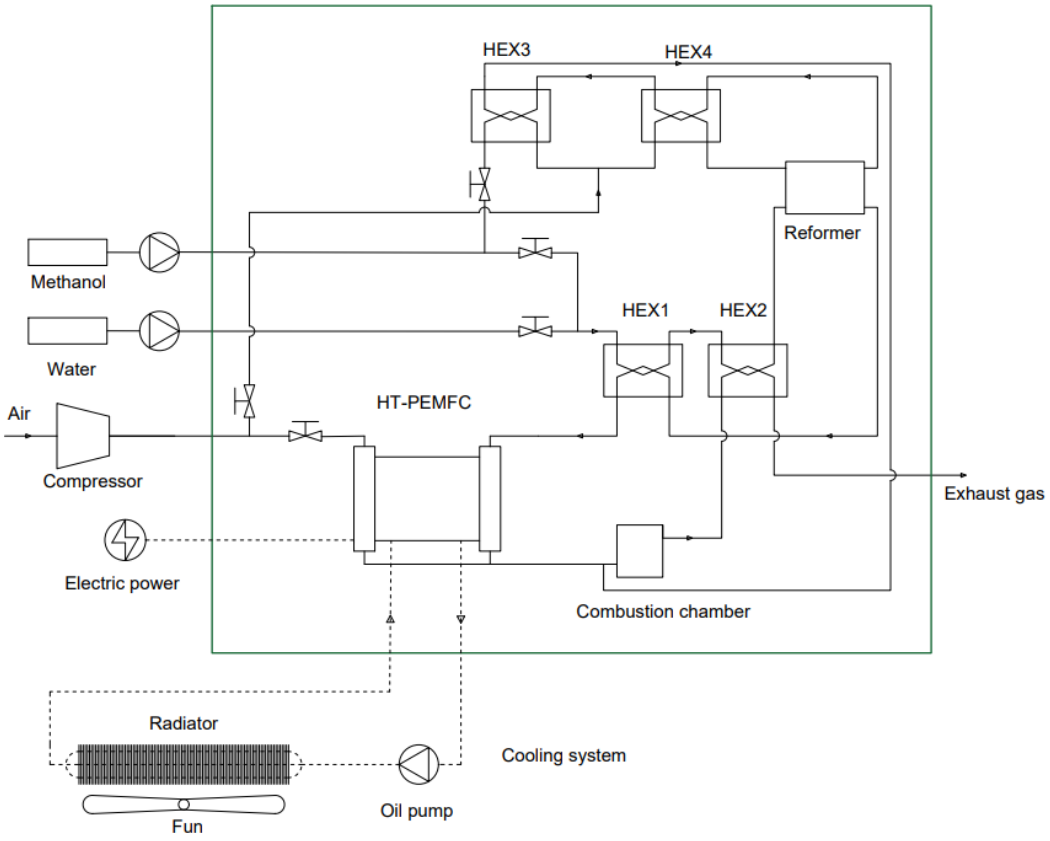

Fig. 2. HT-PEMFC system with the detailed reforming system

The reformer adopts a self-heating micro-channel reformer. Chodba et al. [12] proposed a reformer system used to provide reformer gas to HT PEMFC. The reformer system and gas composition are used for this simulation, assuming the reformed gas composition ratio is constant. The mixture of methanol and air undergoes a self-heating reaction in the oxidation

channel. Fig. 2 shows the internal structure of the reformer, an exothermic oxidation reaction of Methanol (CH_3OH) in a channel parallel with reformer channels can provide the required heat for the endothermic steam reforming reactions; the reaction produces Carbon Dioxide (CO_2) and Water (H_2O). The reaction for total methanol combustion, Total Oxidation of Methanol (TOM), is given in Eq. (28).

$$CH_3OH + 1.5O_2 \rightleftarrows CO_2 + 2H_2O(\Delta H = -725.76\ kJ/mol) \quad (28)$$

The main chemical reactions involved in the Methanol Steam Reforming (MSR) process is as Eq. (29), Methanol Decomposition (MD) is as Eq. (30) and Water-Gas Shift (WGS) and Reverse Water Gas Shift (RWGS) in Eq. (31) [37]:

$$CH_3OH + H_2O \rightleftarrows CO_2 + 3H_2(\Delta H = 49.4\ kJ/mol) \quad (29)$$

$$CH_3OH \rightleftarrows CO + 2H_2(\Delta H = 90.5\ kJ/mol) \quad (30)$$

$$CO + H_2O \rightleftarrows CO_2 + H_2(\Delta H = -41.1\ kJ/mol) \quad (31)$$

The results are for the temperature at 483.5K, pressure at 1atm, H_2O/CH_3OH ratio is 1.1. The molar composition of reformed gas is 61.5% H_2 and 0.5% CO, a more detailed explanation of the calculation process has been provided in the reference [12]. Considering that the pressure almost affects the reactant gas composition and matches the air pressure, the reformed gas pressure is selected as 2atm [38]. Other assumptions about the reformer include ignoring the influence of different loads on the ratio of products.

Considering that the HT-PEMFC and reformer system (in the green line) is an adiabatic system (except HT-PEMFC stack) in Fig. 2, based on the mass balance, the consumption ratio of air, water, and methanol can be obtained.

Assumptions about this system are as follows:

1. The HT-PEMFC stack is adiabatic; it only exchanges heat with the cooling system.
2. The reformed gas enters the fuel cell at a temperature of 448K.
3. The reformer gas composition is constant.
4. The exhaust gas temperature is 393K.

The reaction of the whole system can be regarded as the complete combustion reaction of methanol and the heating of Nitrogen (N_2) and water. The total reaction of the system in Eq. (32):

$$CH_3OH(l) + 1.5(O_2 + 3.7N_2)(g) + aH_2O(l) \rightleftarrows CO_2(g) + (2+a)H_2O(g) + 5.55N_2(g) \quad (32)$$

The system reaction enthalpy is $\Delta H = -599 + 48.9a$ kJ/mol, where a is the ratio of methanol undergoing steam reforming to oxidation. Through stack model calculation, the quality of consumed hydrogen $\dot{m}_{H_2}$, the power output P_{stack}, and the heat removed by the cooling system $q_{cooling} = q_{stack}$ can be known.

Through heat balance, the ratio a and flow rate of methanol $\dot{m}_{methanol}$ ($\mathrm{g\,s^{-1}}$) and air can be calculated using Eq. (33), Eq. (34) and Eq. (35):

$$\frac{\dot{m}_{methanol}}{M_{mathanol}}(-599 + 48.9a) + q_{cooling} + P_{stack} = 0 \quad (33)$$

$$\frac{\dot{m}_{H_2}}{M_{H_2}} = 3a\frac{\dot{m}_{methanol}}{M_{mathanol}} \quad (34)$$

$$1.5\frac{\dot{m}_{methanol}}{M_{mathanol}} = \frac{\dot{m}_{air}}{M_{air}}x_{O_2} \quad (35)$$

Where, $M_{mathanol}$, M_{H_2} and M_{air} are the molar mass of methanol, hydrogen, and air; which are 32 g/mol, 2 g/mol and 28 g/mol respectively. x_{O_2} is the mass fraction of oxygen in the air.

Table 2 shows the parameters of the reformer system [12].

Table 2 Parameters for the reformer system

Parameter	Value	Unit
Length	0.054	m
Diameter	1.5×10^{-3}	m
Catalyst thickness	1×10^{-4}	m

2.3 Cooling system model

The heat from the stack is assumed to be fully dissipated through the cooling system; other dissipation processes such as thermal radiation or exhaust gas are not considered [25]. The stack cooling model is developed to estimate the operating temperature of the fuel cell. Under different working conditions, the fuel cell temperature should be maintained within the designed range. Too high operating temperature causes degradation; too low temperature deteriorates fuel cell performance due to increased activation voltage loss.

2.3.1 Stack cooling

The stack cooling model is developed to estimate the HT-PEMFC stack's heat balance and estimate the fuel cell operating temperature. According to the assumptions, all the heat of the stack is taken away by the cooling system. Based on energy balance, the change of the stack temperature T_{cell} (K) is determined by the heat generation q_{cell} and heat dissipation of the fuel cell through the cooling oil loop as shown in Equation (36):

$$C_{p,cell} m_{cell} \frac{dT_{cell}}{dt} = q_{cell} - C_{p,oil} \dot{m_{oil}} \left(T_{oil,out} - T_{oil,in}\right) \tag{36}$$

Where, $C_{p,cell} m_{cell}$ is the thermal mass of the fuel cell stack (kJ/K). $C_{p,oil}$ is the specific heat

capacity of the cooling water, 2 kJ/kg·K, q_{cell} is the fuel cell heat (kW); $\dot{m_{oil}}$ is the mass flow rate of the cooling oil (kg/s); $T_{oil,out}$ and $T_{oil,in}$ are the stack inlet and stack outlet cooling oil temperature respectively (K).

2.3.2 Radiator

The radiator is used to cool the high-temperature oil from the mixer by ambient air. The intercooler and the radiator are established using the Number of Transfer Unit (NTU) method. This method can calculate the maximum heat exchange between hot fluids (cooling oil) and cold fluids (low-temperature cooling oil). The heat transfer rate of the radiator between the hot fluid and cool fluid q_{heat} (kW) can be calculated as Eq. (37):

$$q_{heat} = \varepsilon C_{min}(T_{hi} - T_{ci}) \tag{37}$$

Where ε is the ratio between the actual heat transfer rate and the maximum possible heat transfer rate. C_{min} is the smaller one of $\dot{m}_{coolfluid}C_{p,coolfluid}$ and $\dot{m}_{hotfluid}C_{p,hotfluid}$ (W/K). T_{hi} is the inlet temperature of hot fluid (K). T_{ci} is the inlet temperature of cool fluid (K). In the counterflow heat exchanger, $\varepsilon = (1 - \exp(-NTU(1 + C)/1 + C)$, $NTU = UA_{ra}/C$ and $C = C_{min}/C_{max}$. U is the overall heat transfer coefficient (W/m^2K). A_{ra} is the heat transfer area of the radiator (m^2). Heat transfer oil is a suitable alternative in high-temperature cooling system due to its higher heat capacity (2 kJ/kg K) and thermal conductivity (0.16 W/m K)[30]. The heat transfer oil is FRAGOLTHERM○R S-15-A.

2.3.3 Oil pump

The oil pump circulates the cooling oil in the cooling system. Considering that the cooling oil is an incompressible liquid, the power of the oil pump can be calculated by Eq. (38):

$$P_{pump} = \Delta P_{pump} \dot{m}_{oil} / \eta_{pump} \tag{38}$$

Where ΔP_{pump} is the pressure difference of the cooling oil passing through the pump, that is, the pressure that needs to be overcome due to the circulation of the cooling oil (kPa). $\dot{m}_{oil}$ is the flow rate of cooling oil (kg/s), η_{pump} the efficiency of pump is 0.6. The pressure drop is gave by loss fitting formula of water-cooled PEMFC as Eq. (39) [39]. The pressure drop caused by the cooling oil ΔP (kPa) when passing through the pipeline can be calculated using Eq. (40). Therefore, the pressure drop of oil is approximated by converting the pressure drop of water, as Eq. (41).

$$\Delta P_{water} = 3.2743 \dot{m}_{water}{}^2 + 5.5977 \dot{m}_{water} \tag{39}$$

$$\Delta P = \frac{64 \mu_{cool}}{v_{cool}} \cdot \frac{L_h}{2 d_h^2} \left(\frac{\dot{m}_{cool}}{\rho_{cool} A_{ch}} \right)^2 \tag{40}$$

$$\Delta P_{oil} = \frac{\mu_{oil} v_{water}}{\mu_{water} v_{oil}} \left(\frac{\dot{m}_{oil} \rho_{water}}{\dot{m}_{water} \rho_{oil}} \right)^2 \Delta P_{water} \tag{41}$$

Where, $\dot{m}_{water}$ is the flow rate of water when using water as the coolant (kg/s), ΔP_{oil} is the pressure drop of oil(kPa), μ_{water} and μ_{oil} are the viscosity of water and oil, 0.37 mPa · s and 1.89 mPa · s. v_{water}/v_{oil} is the ratio of the flow rate of oil and water, which can be written as $\dot{m}_{water} \rho_{oil} / \dot{m}_{oil} \rho_{water}$. ρ_{water} is the density of water, 974kg/m^3; ρ_{oil} is the density of oil, 901kg/m^3[30]. Table 3 shows the parameters of the cooling system [39].

Table 3 Parameters for the cooling system

Parameter	Value	Unit
Radiator		
length	0.7	m

width	0.4	m
Diameter of tube	0.035	m
Fin height	9.15×10^{-3}	m
Louver angle	28	
Louver pitch	1.14×10^{-3}	m
Core Thickness	7.6×10^{-2}	m
Fan		
Blade diameter	0.52	m
Hub diameter	0.2	m
Power	450	W

2.4 Model validation

Fig. 3 (a) and (b) show the single HT-PEMFC fuel cell output voltage at different operating temperatures 423K and 448K compared to experimental results in reference [8]. The error analysis for measured experimental results has not been presented in the reference. Thus, Fig. 3 doesn't show the uncertainty of experimental results. The input parameters for validation of the HT-PEMFC model are listed in Table 4. In Fig. 3 (a), the model result and the experimental data overlap at 5% CO and 10% CO. In the case of pure hydrogen, the model voltage is 0.02V lower than the experimental data on average. When the temperature is 448K, the difference between the simulated voltage and the experimental data is small. Within the range of working current density, the error between model data and experimental data is less than 0.01V.

As shown in Fig. 3, the polarization curves are different when the fuel cell operates at different

CO concentrations. At a current density of 0.5A/cm2, the cell voltage is 0.52V for pure hydrogen. At 5% CO, the cell voltage drops by 0.04V, and when CO increases to 10%, the cell voltage drops by 0.1V. As the proportion of CO increases, the voltage loss decreases faster. Similarly, when the operating temperature is 448K and the current density is 1A/cm2, the cell voltage of pure hydrogen is 0.48V. At 5%CO, the cell voltage drops by 0.01V. At 10%CO, the cell voltage drops by 0.12V.

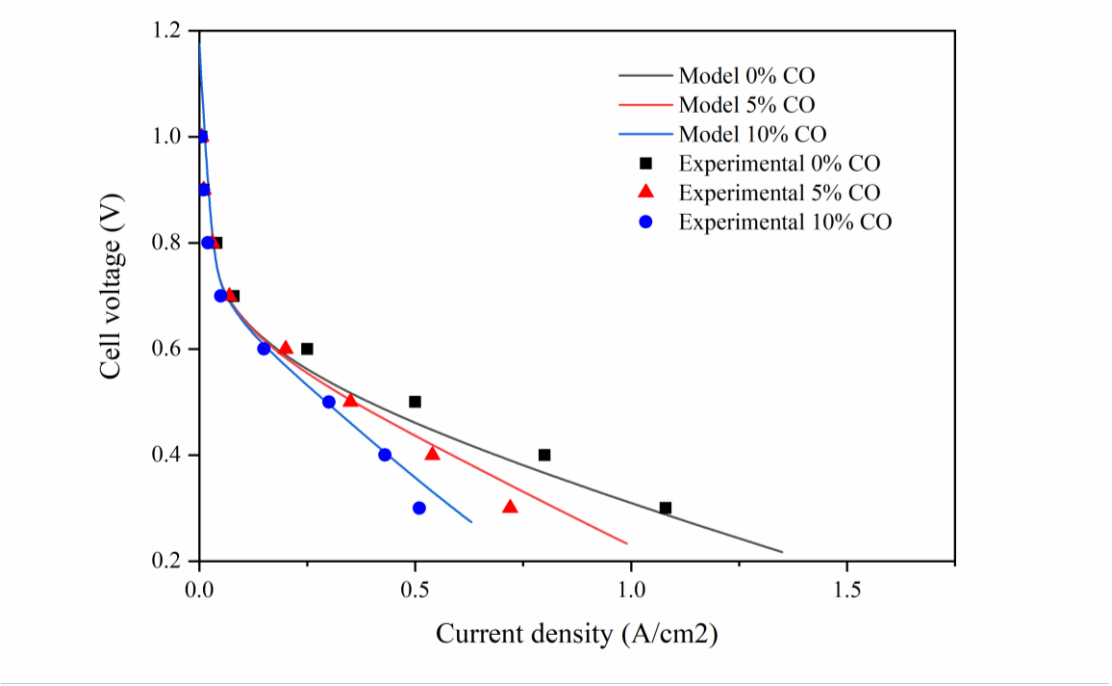

(a) Operating temperature at 423K

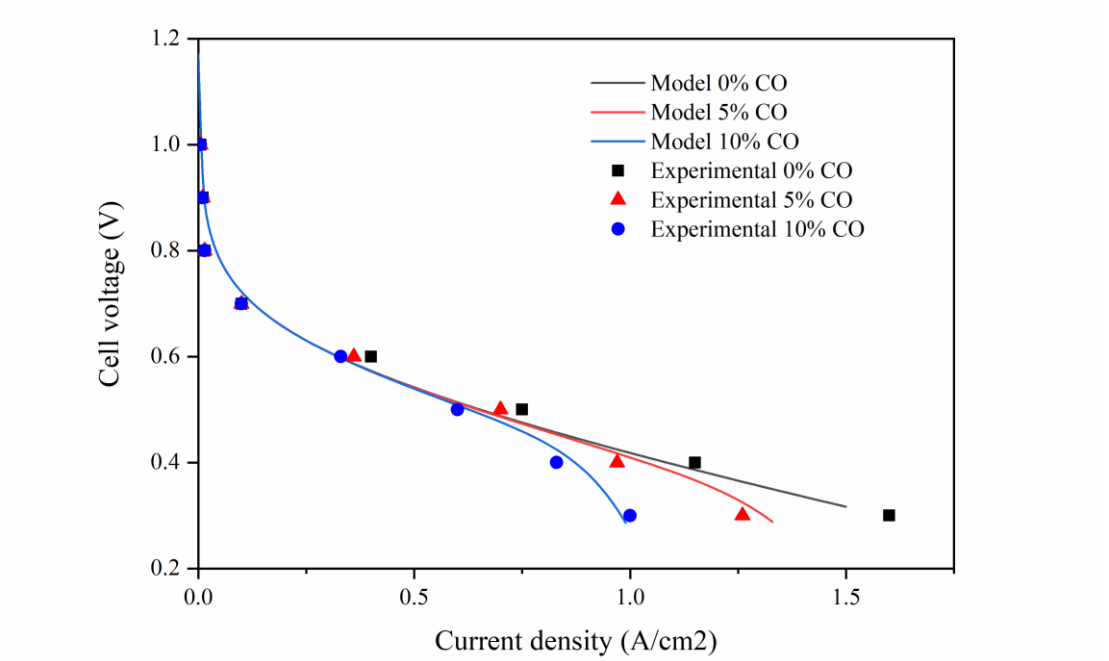

(b) Operating temperature at 448K

Fig. 3. Validation of HT PEMFC model at different %CO and operating temperatures

Table 4 Parameters used in validation of HT-PEMFC

Parameters	**Value**	**Units**
Number of fuel cells, $\boldsymbol{N_{cell}}$	370	N/A
Operating temperature, $\boldsymbol{T_{cell}}$	423, 448	K
Atmospheric temperature, $\boldsymbol{T_{atm}}$	298	K
Current density, $\boldsymbol{I}$	0-1.6	A cm^{-2}
Faraday constant, $\boldsymbol{F}$	96485	C mol^{-1}
Active area, $\boldsymbol{A}$	200	cm^2
Anode inlet gas pressure, $\boldsymbol{P_{anode}}$	2	atm
Cathode inlet gas pressure, $\boldsymbol{P_{cathode}}$	2	atm

Membrane thickness, l_m	4×10^{-5}	m
Anode film thickness, δ_{anode}	2.5×10^{-9}	m
Cathode film thickness, $\delta_{cathode}$	1.48×10^{-9}	m
Anode reference exchange current density, $i_{0,a}^{ref}$	1440	$A\ m^{-2}$
Cathode reference exchange current density, $i_{0,c}^{ref}$	0.0004	$A\ m^{-2}$
Anode catalyst surface area, $a_{c,a}$	64	$m^2\ g^{-1}$
Cathode catalyst surface area, $a_{c,c}$	32.25	$m^2\ g^{-1}$
Anode catalyst loading, $L_{c,a}$	0.0005	$g\ cm^{-2}$
Cathode catalyst loading, $L_{c,c}$	0.0005	$g\ cm^{-2}$
Transfer coefficient at anode, α_a	0.5	N/A
Transfer coefficient at cathode, α_c	0.75	N/A
Reaction order at anode, γa	1	N/A
Reaction order at cathode, γc	1.375	N/A
Anode reference concentration, $C_{ref,a}$	2×10^{-7}	$mol\ cm^{-3}$
Cathode reference concentration, $C_{ref,c}$	4×10^{-7}	$mol\ cm^{-3}$
Anode activation energy, $E_{c,a}$	16900	$J\ mol^{-1}\ K^{-1}$
Cathode activation energy, $E_{c,c}$	72400	$J\ mol^{-1}\ K^{-1}$
Anode reference cell temperature, $T_{ref,a}$	433.15	K
Cathode reference cell temperature, $T_{ref,c}$	373.15	K

The combination of CO and the catalyst on the electrode will cause the catalyst to fail or to lose voltage. As the CO concentration increases, the catalyst combines with more CO, and the

voltage loss increases. When the proportion of CO exceeds 10%, the CO poisoning inhibit on the catalyst and the cell voltage loss rises sharply. At an operating temperature of 448K and a current density of 0.5 A/cm2, the cell voltage of 10% CO is 0.57V, which is 0.25V higher than the cell voltage under the same conditions at the operating temperature 423K. At a temperature of 423K and a current density of 0.5, 10%CO will cause a voltage loss of 0.1V. While at a temperature of 448K, 10%CO will not cause a voltage loss. As the temperature rises, the poisoning effect of CO weakens, and CO and the catalyst on the electrode are more difficult to Combine at a higher temperature. Therefore, at 448K and a current density less than 0.5 A/cm^2, the cell voltage is the same as pure hydrogen. Overall, at the operating temperature of 423-448K and 0%-10%CO, the HT PEMFC model reflects the actual performance.

3. Results and discussions

Section 3 presents the phosphoric acid doped high-temperature proton exchange membrane fuel cell stack's performance for vehicle application. It also discusses the thermal management strategy which enables the balance of heat generation and dissipation within the fuel cell stack. Finally, the oil pump and fan pump are estimated and evaluated.

3.1 Fuel cell stack performance

The performance of a single fuel cell has been validated against the experimental results using parameters presented in Table 4. For applying fuel cell stack in the automotive vehicles, the parameters of the PEMFC stack are shown in Table 5 [9]. The temperature range of 393-453K is the typical operating temperature of HT-PEMFC. The lower boundary temperature of 393K is recommended to avoid the formation of liquid water, while the upper boundary level of 453K

is to avoid furious degradation[40]. 448K is chosen as the operating temperature of the fuel cell, which is lower than the damage temperature of the membrane and has a higher voltage than the operating temperature of 423K.

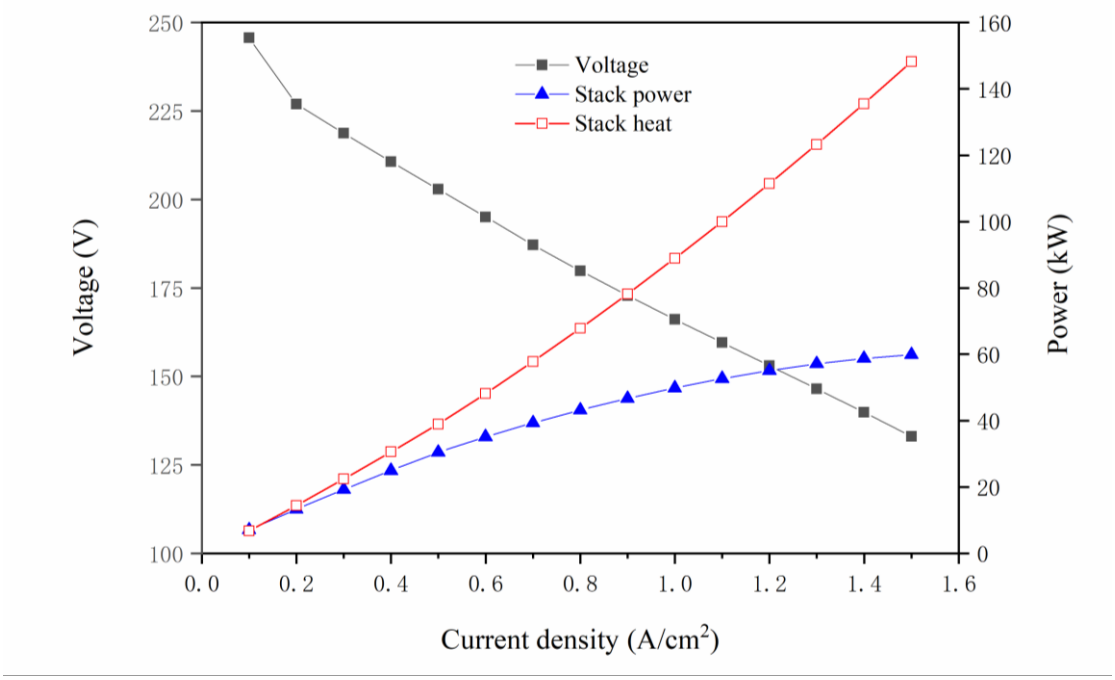

Fig. 4. HT-PEMFC output characteristic curve at 448K

Fig. 4 shows the characteristics of HT-PEMFC, voltage, heat generation, and power at different current densities at operating temperatures. At 0.1A/cm^2, the heat production and the power are 7kW, the heat to power ratio is 1. At 0.5A/cm^2, the heat production is 39kW, the power is 30kW, and the heat to power ratio is 1.3. At 1.5A/cm^2, the heat production is 148kW, the rated power is 60kW, and the heat to power ratio is 2.5. When the current density increases from 0.5A/cm^2 to 1A/cm^2, the heat to power ratio increases from 1.3 to 2.5. The smaller the heat-to-power ratio, the higher the efficiency of the fuel cell, so 0.5 A/cm^2 is selected as the rated current density. At this current density, the poisoning effect of CO is low, and the heat to power ratio is low.

Table 5 Parameters for the stack model

Parameters	**Value**	**Units**
Number of fuel cells, N_{cell}	370	N/A
Operating temperature, T_{cell}	448	K
Atmospheric temperature, T_{atm}	298	K
Current density, I	0-1.6	A cm^{-2}
Faraday constant, F	96485	C mol^{-1}
Active area, A	300	cm^2
Anode inlet gas pressure, P_{anode}	2	atm
Cathode inlet gas pressure, $P_{cathode}$	2	atm
Membrane thickness, l_m	4×10^{-5}	m
Anode film thickness, δ_{anode}	2.5×10^{-9}	m
Cathode film thickness, $\delta_{cathode}$	1.48×10^{-9}	m
Anode reference exchange current density, $i_{0,a}^{ref}$	1440	A m^{-2}
Cathode reference exchange current density, $i_{0,c}^{ref}$	0.0004	A m^{-2}
Anode catalyst surface area, $a_{c,a}$	64	m^2 g^{-1}
Cathode catalyst surface area, $a_{c,c}$	32.25	m^2 g^{-1}
Anode catalyst loading, $L_{c,a}$	0.0002	g cm^{-2}
Cathode catalyst loading, $L_{c,c}$	0.0004	g cm^{-2}
Transfer coefficient at anode, α_a	0.5	N/A
Transfer coefficient at cathode, α_c	0.75	N/A
Reaction order at anode, γa	1	N/A

Reaction order at cathode, $\boldsymbol{\gamma c}$	1.375	N/A
Anode reference concentration, $\boldsymbol{C_{ref,a}}$	2×10^{-7}	mol cm^{-3}
Cathode reference concentration, $\boldsymbol{C_{ref,c}}$	4×10^{-7}	mol cm^{-3}
Anode activation energy, $\boldsymbol{E_{c,a}}$	16900	J mol^{-1} K^{-1}
Cathode activation energy, $\boldsymbol{E_{c,c}}$	72400	J mol^{-1} K^{-1}
Anode reference cell temperature, $\boldsymbol{T_{ref,a}}$	433.15	K
Cathode reference cell temperature, $\boldsymbol{T_{ref,c}}$	373.15	K

3.2 Thermal management

Varying operating temperatures and uneven temperature distribution cause degradation [1] and shorten fuel cell life span. The performance of the fuel cell increases with the increase of the operating temperature; it still needs to be controlled within a reasonable range (<453K) to avoid degradation. Therefore, the inlet oil temperature is selected between 435-445K to ensure this. The temperature difference between the inlet and outlet cooling oil is suggested to be less than 8K, and the maximum operating temperature is 453K [41]. Regulations of inlet cooling oil temperature and cooling oil flow rate is suggested to maintain the internal thermal balance of the HT-PEMFC [42]. Considering that the pump power consumption increases when the flow rate is too large, so the flow rate is controlled below 5kg/s.

Fig. 5 presents the outlet cooling oil temperature T_{out} and temperature difference between inlet and outlet cooling oil $T_{out} - T_{in}$ at various cooling oil flow rate and inlet cooling oil temperature. When the current density is 0.3 A/cm^2 and 0.5 A/cm^2, the changing trend of the outlet cooling oil temperature and the temperature difference is similar.

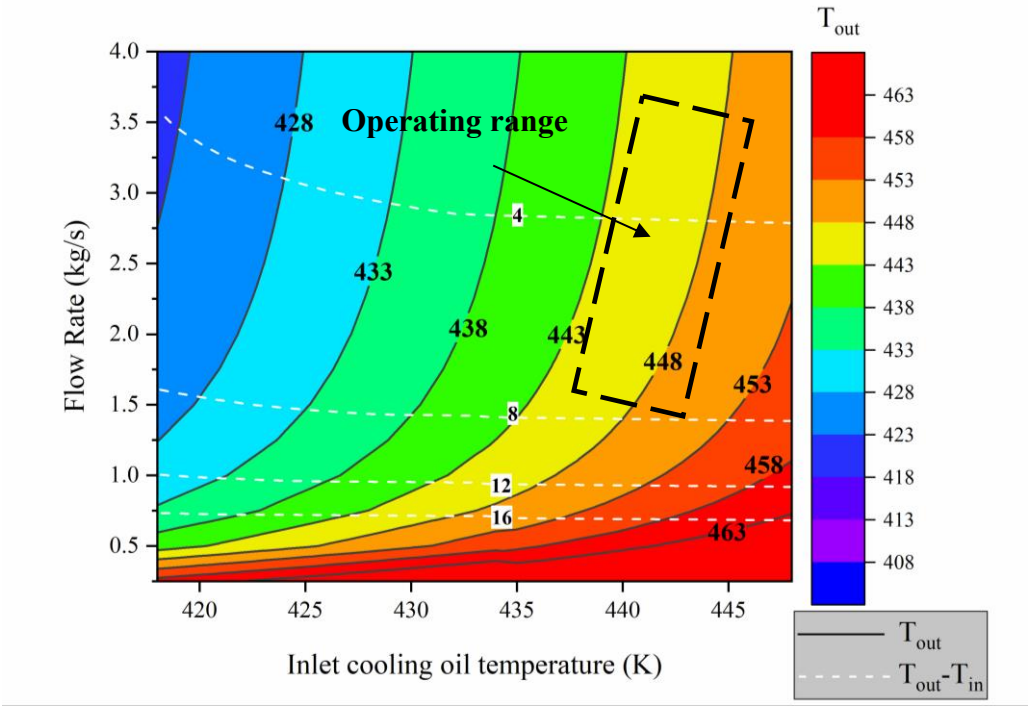

(a) Current density at 0.3A/cm^2

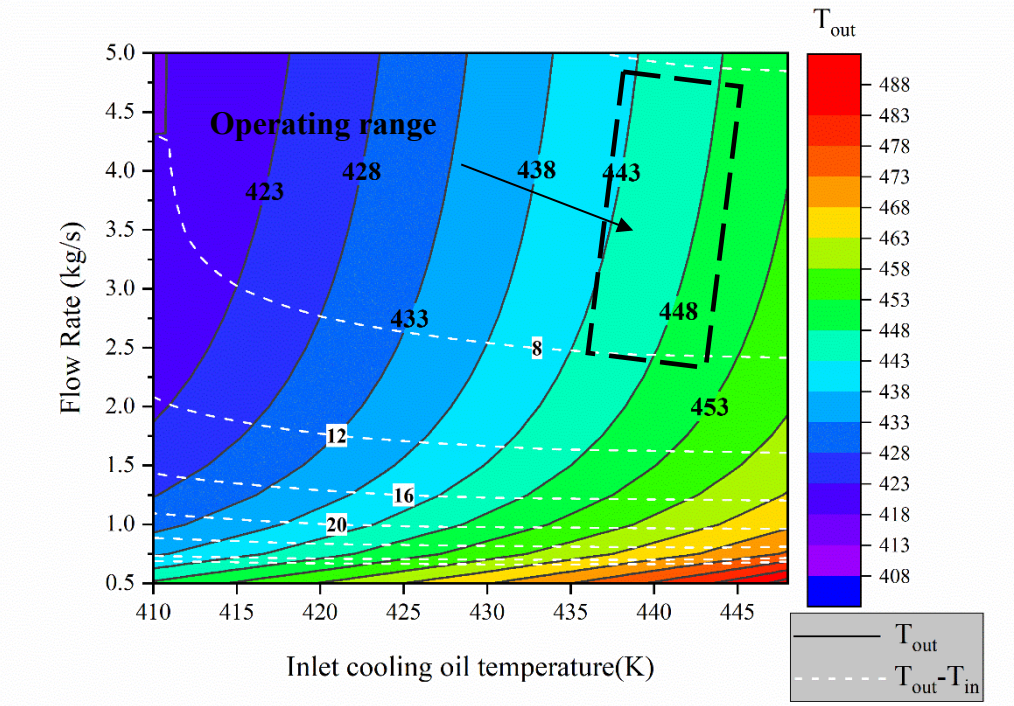

(b) Current density at 0.5A/cm^2

Fig. 5 Outlet cooling oil temperature and temperature difference at the various inlet cooling

oil temperature and cooling oil flow rate

In Fig. 5(a), the temperature difference only changes with flow rate. At a flow rate of 1kg/s, the temperature difference is 12K, and at a flow rate of 1.5kg/s, the temperature difference is 8K. The outlet cooling oil temperature should be as close as possible to the operating temperature of 448K and adjust the flow rate to meet the heat dissipation requirements. The black dotted box in the figure shows the range of inlet cooling oil temperature and oil flow rate. As mentioned above, the temperature difference between inlet and outlet cooling oil should be less than 8K, and the maximum temperature should not exceed 458K. For the current density of 0.3 A/cm^2, the inlet cooling oil temperature range is 437-446K, and the flow rate range is 1.5-3.5kg/s. For the current density of 0.5 A/cm^2, the inlet cooling oil temperature range is 435-445K, and the flow rate range is 2.5-5kg/s.

3.3 Heat generation and dissipation of fuel cell stack

Fig. 6 (a) and (b) show the HT-PEMFC heat generation at different inlet cooling oil temperatures. At the inlet temperature of 430K, when the flow rate changes from 1.5kg/s to 3.5kg/s, the stack heat generation increases from 39.5kW to 41.2kW. When the inlet temperature is 440K, the flow rate changes from 1.5kg/s to 3.5kg/s, the heat generated by the stack increases from 38.7kW to 39.2kW.

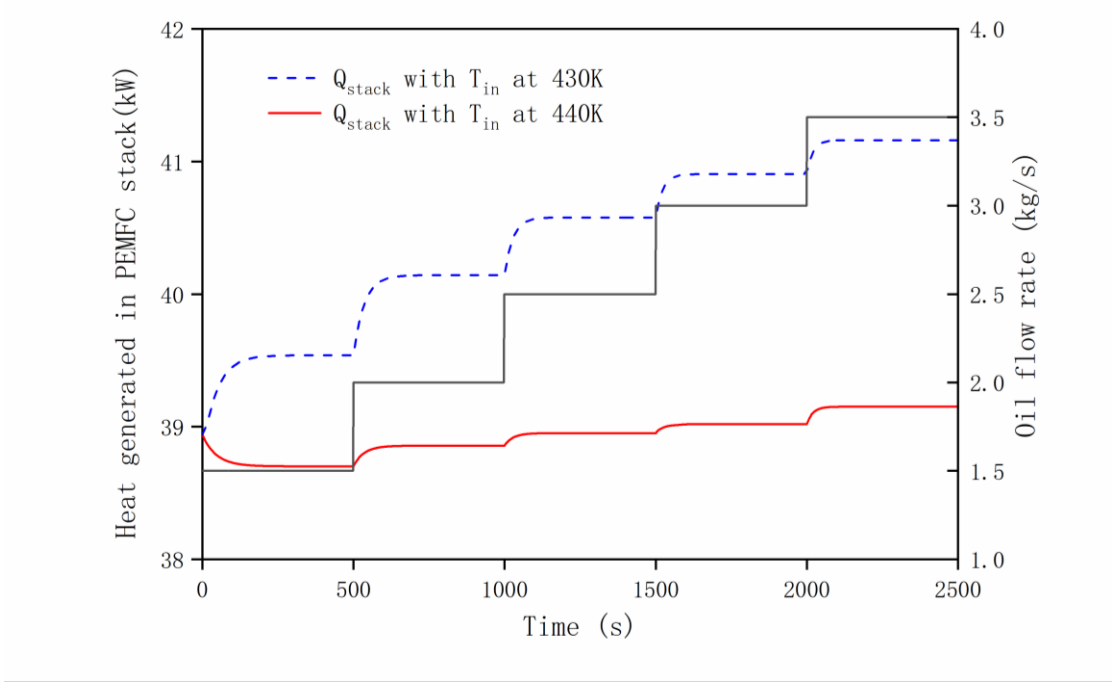

(a) PEMFC stack heat generation

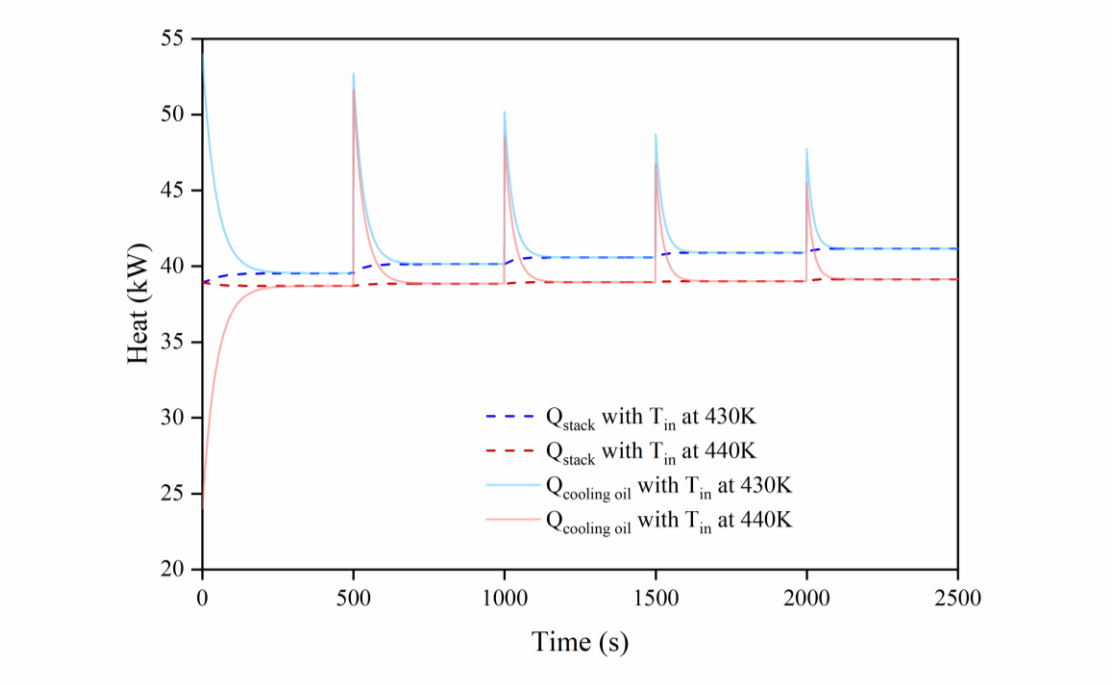

(b) Heat dissipation through the cooling system

Fig. 6 Stack heat generation and heat dissipation at different stack inlet cooling oil temperature (430K and 440K)

As the flow rate increases, the heat production also rises. This is because cooling oil takes away more heat, the operating temperature of the fuel cell drops, and the efficiency drops, leading to increased heat production. In Fig. 6(b), the heating peak caused by the oil flow change at the inlet oil temperature of 440K is less than 430K which is 52kW compared to 51kW at 500s. To avoid the sudden rise in heat production, a higher inlet cooling oil temperature and a more significant flow rate should be selected, such as 440K and 3.5kg/s.

3.4 Oil pump and fan power

Operated fan and pump consume energy to regulate the cooling oil flow rate and inlet cooling oil temperature for the thermal management of the stack. The energy efficiency $\eta_{net} = P_{net}/P_{stack}$ and net power $P_{net} = P_{stack} - P_{pump} - P_{fan}$ are calculated to evaluate fan and pump power ratio compared to stack output power at various stack operating conditions. The calculations quantify the impact of cooling oil flow rate regulations and stack inlet cooling oil temperature on the stack performance. Fig. 7 shows the net power output and energy efficiency at the various stack inlet cooling oil temperature and cooling oil flow rate at 0.3A/cm^2 and 0.5A/cm^2. Operating the fuel cell at a higher stack inlet cooling oil temperature and a relatively lower cooling oil flow rate is suggested to minimize the fan power and oil pump power consumption.

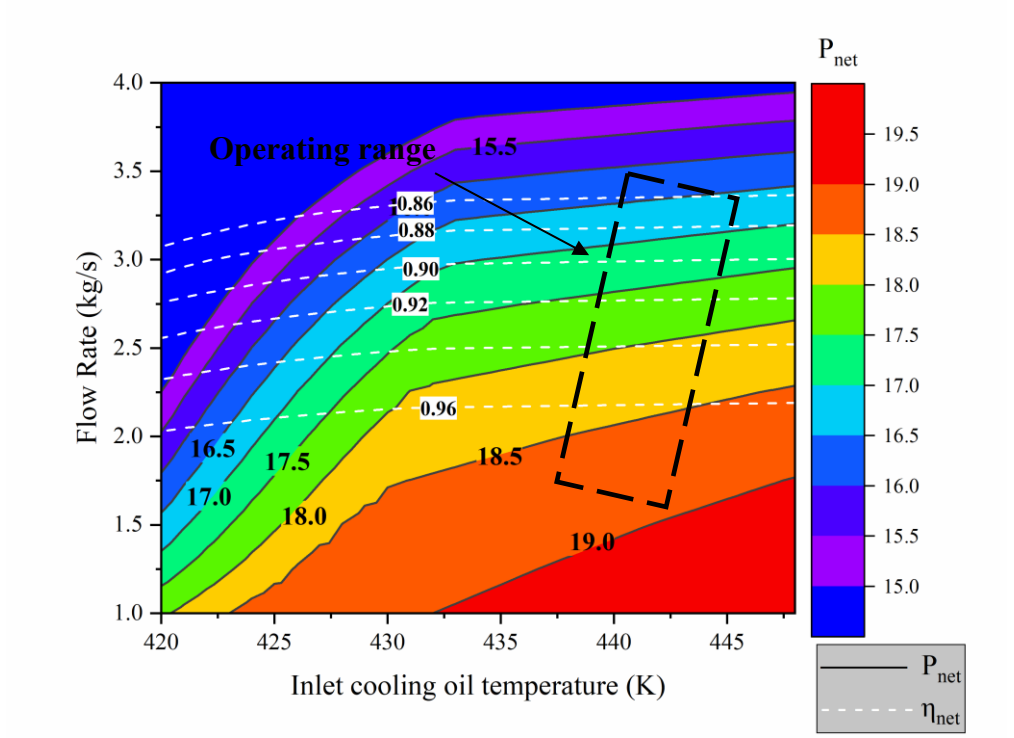

(a) Working at current density 0.3A/cm^2

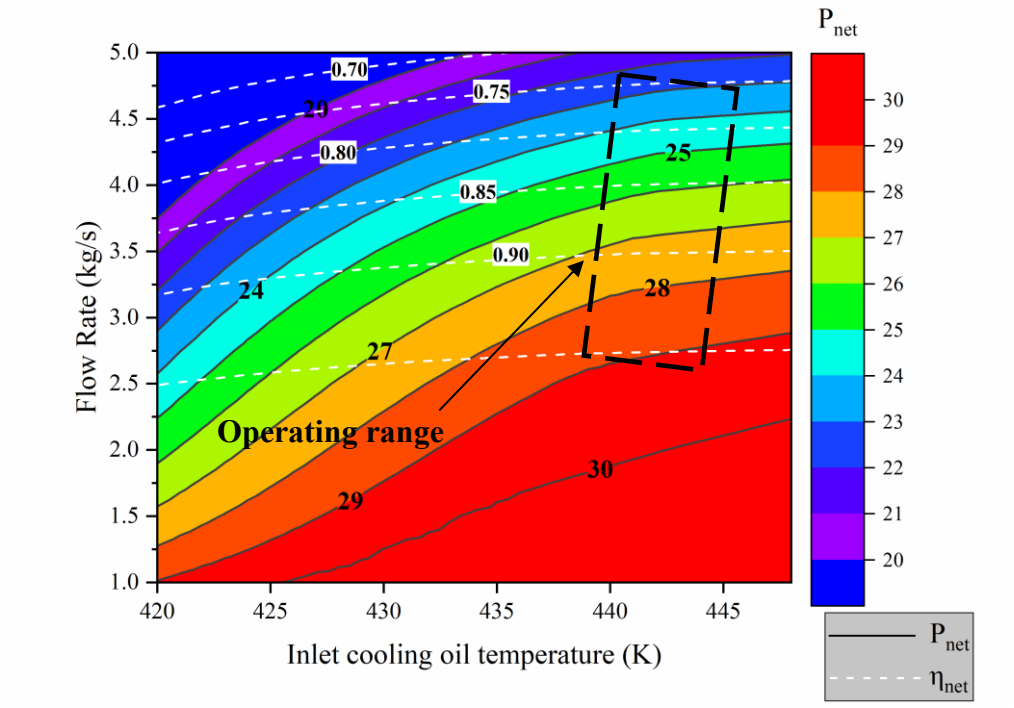

(a) Working at current density 0.5A/cm^2

Fig. 7 Net power output P_{net} and energy efficiency η_{net} at the various stack inlet cooling

oil temperature and cooling oil flow rate

In summary, for the thermal management of the PEMFC stack for automotive vehicles, several constraints must be considered: differences in stack inlet and outlet cooling oil temperature, stack temperature, fan, and pump power consumptions. It is recommended that the inlet cooling oil should be maintained at (435-440K) and change the cooling oil flow rate to meet the heat dissipation requirements under variable working conditions.

4. Conclusions

This paper presents a simulation model of an oil-cooled phosphoric acid doped HT PEMFC stack for automotive applications. The heat dissipation requirement for the PEMFC stack is analyzed. Analysis results show that increasing operating temperature to 448K reduced the extra stack heat generation caused by CO poisoning. It is suggested to keep the inlet cooling oil temperature constant within the range of 435-445K and adjust the cooling oil flow rate within 2.5-5kg/s to maintain the stack's thermal balance. Due to the significant temperature difference between the fuel cell and the external environment (> 150K), 39kW recoverable waste heat is available. Effective waste heat recovery could be explored for future work. Preheating the reforming reactant is a way to recover waste heat, reducing the fuel required for reforming.

To the authors' knowledge, this is a first-of-a-kind analysis related to modeling and investigation to verify the feasibility of the methanol-fueled high-temperature proton exchange membrane fuel cell (30kW) with an oil cooling system applied in an automotive application. This research provides the theoretical background for modeling and detailed analysis of vehicle integrated thermal management systems for HT PEMFC vehicles, which may be used as a

reference in future research.

This work paves the way for developing a fuel cell electric hybrid vehicle powered by phosphoric acid-doped HT PEMFC. HT PEMFC presents higher carbon monoxide tolerance; they can use liquid fuel such as methanol, ethyl alcohol. It is a promising technology to be applied for automotive vehicles and further developed. This will promote the decarbonization of the transportation industry by implementing hydrogen technologies. Future work will be devoted to developing and implementing an intelligent energy/thermal management strategy for the HT PEMFC/electric hybrid vehicle to achieve optimized techno-economic-environmental performance.

Acknowledgement

This work was supported by the National Key Research and Development Program of China (No.2018YFC0810000), the National Natural Science Foundation of China (No. 51776144), Natural Science Foundation of Hubei Province (No. 2020CFA040) and Wuhan Applied Foundational Frontier Project (No. 2020010601012205).

References

[1] Rosli RE, Sulong AB, Daud WRW, Zulkifley MA, Husaini T, Rosli MI, et al. A review of high-temperature proton exchange membrane fuel cell (HT-PEMFC) system. International Journal of Hydrogen Energy. 2017;42:9293-314.

[2] Liu YF, Lehnert W, Janßen H, Samsun RC. A review of high-temperature polymer electrolyte membrane fuel-cell (HT-PEMFC)-based auxiliary power units for diesel-powered road vehicles. Journal of Power Sources. 2016; 311: 91-102.

[3] Zhang J, Xie Z, Zhang J, Tang Y, Song C, Navessin T, et al. High temperature PEM fuel cells. Journal of Power Sources. 2006;160:872-91.

[4] Vogel JA. Development of polybenzimidazole-based high-temperature membrane and electrode assemblies for stationary and automotive applications. Plug Power Inc; 2008.

[5] Millo F, Caputo S, Piu A. Analysis of a HT-PEMFC range extender for a light duty full electric vehicle (LD-FEV). International Journal of Hydrogen Energy. 2016;41:16489-98.

[6] Bargal MHS, Abdelkareem MAA, Tao Q, Li J, Shi J, Wang Y. Liquid cooling techniques in proton exchange membrane fuel cell stacks: A detailed survey. Alexandria Engineering Journal. 2020;59:635-55.

[7] Li YJ, Ma ZS, Zheng M, Li DX, et al. Performance analysis and optimization of a high-temperature PEMFC vehicle based on particle swarm optimization algorithm. Membranes. 2021; 11(9):691.

[8] Li Q, He R, Gao J-A, Jensen JO, Bjerrum NJ. The CO Poisoning effect in PEMFCs operational at temperatures up to 200°C. Journal of The Electrochemical Society. 2003;150:A1599.

[9] Mamlouk M, Sousa T, Scott K. A high temperature polymer electrolyte membrane fuel cell model for reformate gas. International Journal of Electrochemistry. 2011;2011.

[10] Du X, Shen Y, Yang L, Shi Y, Yang Y. Experiments on hydrogen production from methanol steam reforming in the microchannel reactor. International Journal of Hydrogen Energy. 2012;37:12271-80.

[11] Reuse P, Renken A, Haas-Santo K, Görke O, Schubert K. Hydrogen production for fuel

cell application in an autothermal micro-channel reactor. Chemical Engineering Journal. 2004;101:133-41.

[12] Chodba A, Sharifzadeh M, Rashtchian D. Integrated and inherently safe design and operation of a mobile power generation: Process intensification through microreactor reformer and HT-PEMFC. International Journal of Hydrogen Energy. 2021;46:23839-54.

[13] Authayanun S, Mamlouk M, Arpornwichanop A. Maximizing the efficiency of a HT-PEMFC system integrated with glycerol reformer. International Journal of Hydrogen Energy. 2012;37:6808-17.

[14] Suwanmanee U, Saebea D, Hacker V, Assabumrungrat S, Arpornwichanop A, Authayanun S. Conceptual design and life cycle assessment of decentralized power generation by HT-PEMFC system with sorption enhanced water gas shift loop. Energy Conversion and Management. 2018;171:20-30.

[15] Korsgaard AR, Nielsen MP, Kær SK. Part one: A novel model of HTPEM-based micro-combined heat and power fuel cell system. International Journal of Hydrogen Energy. 2008;33:1909-20.

[16] Kandlikar SG, Lu ZJ. Thermal management issues in a PEMFC stack - A brief review of current status. Applied Thermal Engineering. 2009; 29 (7): 1276-1280.

[17] Xu JM, Zhang CZ, Fan RJ, Bao HH, etc. Modelling and control of vehicle integrated thermal management system of PEM fuel cell vehicle. Energy. 2020; 199: 117495.

[18] Lim IS, Park JY, Choi EJ, Kim MS. Efficient fault diagnosis method of PEMFC thermal management system for various current densities. International Journal of Hydrogen Energy.

2021; 46(2):2543-2554.

[19] Yan WM, Zeng MS, Yang TF, Chen CY, et al. Performance improvement of air-breathing proton exchange membrane fuel cell stacks by thermal management. International Journal of Hydrogen Energy. 2020; 45:22324-22339.

[20] Yu S, Jung D. Thermal management strategy for a proton exchange membrane fuel cell system with a large active cell area. Renewable Energy. 2008;33:2540-8.

[21] Hosseinzadeh E, Rokni M, Rabbani A, Mortensen HH. Thermal and water management of low temperature Proton Exchange Membrane Fuel Cell in fork-lift truck power system. Applied Energy. 2013;104:434-44.

[22] Yu S, Jung D. A study of operation strategy of cooling module with dynamic fuel cell system model for transportation application. Renewable Energy. 2010;35:2525-32.

[23] Li D, Li C, Gao Z, Jin Q. On active disturbance rejection in temperature regulation of the proton exchange membrane fuel cells. Journal of Power Sources. 2015;283:452-63.

[24] Binrui W, Yinglian J, Hong X, Ling W. Temperature control of PEM fuel cell stack application on robot using fuzzy incremental PID. 2009 Chinese Control and Decision Conference: IEEE; 2009. p. 3293-7.

[25] Cheng S, Fang C, Xu L, Li J, Ouyang M. Model-based temperature regulation of a PEM fuel cell system on a city bus. International Journal of Hydrogen Energy. 2015;40:13566-75.

[26] Baroutaji A, Arjunan A, Ramadan M, Robinson J et al. Advacned and prospects of thermal management and waste heat recovery of PEMFC. International Journal of Thermofluids. 2021; 9: 100064.

[27] Sasiwimonrit K and Chang WC. Thermal management of high temperature polymer electrolyte membrane fuel cells by using flattened heat pipes. Thermal Science. 2021; 25 (4):2411-2423.

[28] Reddy HE, Jayanti S. Thermal management strategies for a 1 kWe stack of a high temperature proton exchange membrane fuel cell. Applied Thermal Engineering. 2012;48:465-75.

[29] Renau J, Barroso J, Lozano A, Nueno A, Sánchez F, Martín J, et al. Design and manufacture of a high-temperature PEMFC and its cooling system to power a lightweight UAV for a high altitude mission. International Journal of Hydrogen Energy. 2016;41:19702-12.

[30] Supra J, Janßen H, Lehnert W, Stolten D. Temperature distribution in a liquid-cooled HT-PEFC stack. International Journal of Hydrogen Energy. 2013;38:1943-51.

[31] Jo A, Oh K, Lee J, Han D, Kim D, Kim J, et al. Modeling and analysis of a 5 kWe HT-PEMFC system for residential heat and power generation. International Journal of Hydrogen Energy. 2017;42:1698-714.

[32] Scholta J, Messerschmidt M, Jörissen L, Hartnig C. Externally cooled high temperature polymer electrolyte membrane fuel cell stack. Journal of Power Sources. 2009;190:83-5.

[33] Song T-W, Choi K-H, Kim J-R, Yi JS. Pumpless thermal management of water-cooled high-temperature proton exchange membrane fuel cells. Journal of Power Sources. 2011;196:4671-9.

[34] Cheddie D, Munroe NJEC, Management. Mathematical model of a PEMFC using a PBI membrane. 2006;47:1490-504.

[35] Weng D, Wainright JS, Landau U, Savinell RF. Electro-osmotic drag coefficient of water and methanol in polymer electrolytes at elevated temperatures. Journal of The Electrochemical Society. 1996;143:1260-3.

[36] Klinedinst K, Bett JAS, Macdonald J, Stonehart P. Oxygen solubility and diffusivity in hot concentrated H3PO4. Journal of Electroanalytical Chemistry and Interfacial Electrochemistry. 1974;57:281-9.

[37] Thattarathody R, Sheintuch M. Kinetics and dynamics of methanol steam reforming on CuO/ZnO/alumina catalyst. Applied Catalysis A: General. 2017;540:47-56.

[38] Özcan O, Akın AN. Thermodynamic analysis of methanol steam reforming to produce hydrogen for HT-PEMFC: An optimization study. International Journal of Hydrogen Energy. 2019;44:14117-26.

[39] Yu S, Jung DJRe. A study of operation strategy of cooling module with dynamic fuel cell system model for transportation application. 2010;35:2525-32.

[40] Reichman S, Ulus A, Peled EJJoTES. PTFE-based solid polymer electrolyte membrane for high-temperature fuel cell applications. 2007;154:B327.

[41] Scholta J, Zhang W, Jörissen L, Lehnert W. Conceptual design for an externally cooled HT-PEMFC stack. ECS Transactions. 2019;12:113-8.

[42] Xing L, Chang HW, Zhu RQ, Wang T, Zou QF, Xiang WT, Tu ZK. Thermal analysis and management of proton exchange membrane fuel cell stack for automotive vehicle. International Journal of Hydrogen Energy. 2021; 46 (64): 32665-32675.